Interaction and Stability of Periodic and Localized Structures in Optical Bistable Systems

Mustapha Tlidi, Andrei G. Vladimirov, and Paul Mandel, *Member, IEEE*

Invited Paper

***Abstract*—We analytically and numerically study the role of the homogeneous zero mode on the interaction between two modulational instabilities. Periodic and localized structures (LSs) are considered in two transverse dimensions. We consider a real-order parameter description for a passive optical cavity driven by an external coherent field, valid close to the onset of optical bistability. A global description of pattern formation in both monostable and bistable regimes is given. We show that the interaction between the modulational modes and the zero mode modifies the existence and the stability of diffractive patterns. In particular, this interaction induces a coexistence between two different types of phase locked hexagonal structures. We also consider the interaction between two separated LSs. An analytical expression for the interaction potential in terms of modified Bessel functions is derived. Numerical simulations confirm the analytical predictions.**

***Index Terms*—Cavity solitons, localized structures, periodic patterns, spatial modulational instability, stability of interacting solitons.**

I. Introduction

DRIVEN optical cavities filled with nonlinear media are the basic configuration in transverse nonlinear optics. More specifically, analytical studies have demonstrated that when diffraction competes with nonlinearity, the homogeneous response is destabilized and allows for the spontaneous formation of self-organized or ordered patterns [1], [2]. Two-dimensional (2-D) nonlinear cavities have been shown to sustain the stable periodic patterns such as hexagons and/or stripes that emerge from the modulational (Turing) instability. (For overviews on this topic, see [3]–[9].) Important examples of stripe and hexagon formations and competition have been reported in various optical systems: Kerr media [10], [11], passive systems [12]–[16], liquid-crystal light valve with feedback [17], counterpropagating beams in a nonlinear medium [18], [19], spin-$1/2$ atomic systems [20], quadratic media [21]–[25], bulk and quantum-well GaAlAs microresonators [26], and active media [27]–[29].

Manuscript received June 14, 2002; revised October 21, 2002. This research was supported in part by the Fonds National de la Recherche Scientifique, by the InterUniversity Attraction Pole program of the Belgian government, and by the European Science Foundation.

M. Tlidi and P. Mandel are with the Theoretical Nonlinear Optics Group, Université Libre de Bruxelles, B-1050 Bruxelles, Belgium.

A. G. Vladimirov is with the Physics Faculty, St. Petersburg State University, 198904 St. Petersburg, Russia, and also with the Weierstrass Institute for Applied Analysis and Stochastics, D-10117 Berlin, Germany.

Digital Object Identifier 10.1109/JQE.2002.807193

Up to now, analytical analysis of pattern formation in nonlinear optical systems has been restricted to the weakly nonlinear regime, where the stationary response is a single-valued function of the input field intensity. In this case, above the modulational instability threshold there exists a band of linearly unstable transverse modes bounded from below by a nonzero wavenumber. The linear growth rate of the zero mode is then negative and the zero mode is damped. As a consequence, the amplitude of this mode coincides with the homogeneous steady state (HSS). At the bistability threshold, that mode is only marginally stable. However, when the system displays bistability, the homogeneous zero mode is included in the linearly unstable transverse modes. The zero mode then becomes an active mode, and will modify not only the domain of existence of the emerging 2-D transverse structures, but also their stability. Such an effect has been studied in one dimension in a normally dispersive all-fiber ring cavity [30]. In that theoretical study, diffraction is replaced by chromatic dispersion, i.e., the intracavity field is spatially stabilized by using a guided-wave structure. The role of the zero-homogeneous mode in pattern formation has also been reported in other nonlinear systems: for the one-dimensional (1-D) Kuramoto–Sivashinsky equation, modeling longitudinal seismic waves in a viscoelastic medium [31] and in reaction-diffusion systems [32]. More recently, we have shown that resonant interaction between the homogeneous zero mode and the modulational mode prevents the stabilization of tetrahedral optical dissipative crystals [33].

To investigate such an interaction, we consider a passive cavity with plane mirrors filled by a resonant two-level medium, and driven by an injected plane wave beam. We assume weak dispersion, where the dynamics is described by a Swift– Hohenberg (SH) equation [34], [35]. The SH model has been derived for many other problems in optics. In particular, close to the threshold for the signal generation, the nonlinear dynamics of the intracavity degenerate optical parametric oscillator and degenerate four-wave mixing are described by a SH equation [36], [37]. More recently, a SH equation has been derived for other classes of nonlinear systems that involve polarization degrees of freedom due to the birefringence of the $\chi^{(2)}$ crystal, namely, intracavity type II second harmonic generation [38]. The SH equation constitutes a paradigm for the study of both periodical and localized patterns formation.

The aim of this paper is twofold. First, it is to clarify the global nonlinear description of the interaction between two subcrit-

ical modulational instabilities and the homogeneous zero mode. Second, it is to study the implication of these interactions on the formation of both bright and dark localized structures (LSs). Throughout this paper, we focus on solutions in two transverse dimensions. Note that LSs are also called cavity solitons, spatial solitons, transverse solitons, or autosolitons, depending on the authors.

Stationary LSs can be observed in optical nonlinear devices where the spatial coupling is provided by diffraction, which affects both the amplitude and the phase of a light wave. This field is now attracting growing interest in optics because of its potential application in information technology. In particular, localized pulses could be used as "bits" for parallel information storage and processing. LSs have been predicted in 1-D bistable systems [39]–[42]. These solutions were interpreted as switching waves connecting two stable branches of the homogeneous response curve. Later, it was shown that the existence of an LS does not require bistable behavior of the spatially homogeneous solutions. They can be stable in the monostable regime where a single homogeneous steady state exhibits a subcritical modulational instability [43]. The 2-D LS appear as bright or dark spots in the profile of intracavity field amplitude. They can be either spatially independent and randomly distributed, or form clusters leading to well-defined spatial patterns in the transverse plane, orthogonal to the propagation axis [43]. Various mean field models have been developed to describe the spatial confinement of light leading to the formation of LS: in purely dispersive two-level media [44], [45], binary-phase and feedback mirror systems [46], quadratic media [38], [47]–[50], semiconductor devices [51]–[54], spin-$1/2$ atomic systems [55], and in active media [56]–[59].

LSs can exhibit periodic oscillations [58]–[64] or chaotic oscillations [65] in time. Recently, experimental observations of localized patterns in a variety of nonlinear optical devices has stimulated further the interest in transverse nonlinear optics, such as in a vertical-cavity semiconductor microresonator, which consists of an active layer sandwiched between Bragg mirrors [66]–[68], in a liquid crystal (LC) light valve with feedback composed by a nematic LC cell followed by a mirror and a layer of photorefractive materials [69], [70], and in a sodium vapor feedback mirror system [71].

In this paper, we show how unstable nontrivial solutions which emerge from both modulational bifurcation points are connected to the stable self-organized structures. We also show that the interaction between the modulational modes and the zero mode induces a bistable behavior between two types of phase-locked hexagonal structures. We systematically compare numerical simulations and the analytical results. This analysis is motivated by the fact that the occurrence of spatially periodic patterns is a prerequisite for the emergence of LSs. However, to envisage applications of LS, a number of problems must be addressed. Each individual localized structure has an oscillatory tail. Two or more LSs will interact through their overlapping tails if they are close enough. Using an asymptotic approach similar to that proposed in [72] and [73], we show for the first time that the interaction potential between two LS in the SH equation can be derived explicitly in terms of modified Bessel functions that describe the asymptotic behavior of the LS tail. A similar analysis has been performed for the bright LS in lasers with a saturable absorber [74] and for a purely absorptive cavity [75], both described by a Ginzburg–Landau type of equation with a saturable nonlinearity.

The paper is organized as follows. After briefly introducing the SH model equation for passive diffractive systems (Section II), we present the analytical study of the interaction between the modulational and the zero modes (Section III). The implications of this interaction in the formation of LSs are considered in Section IV. In the last part (Section V), we study analytically and numerically the interaction between LSs. We conclude in Section VI.

II. Swift–ohenberg Model

We consider a ring cavity filled with two-level atoms without population inversion, and driven by a coherent plane-wave injected signal. We focus on the nascent optical bistability regime centered around the critical point where the output versus input characteristics has only one point with an infinite slope. At the critical point, the cooperativity parameter and the normalized input field are $c_c = 4(1+\Delta^2)$ and $y_c = 3(1+\Delta^2)\sqrt{3}$, respectively. The HSS of the Maxwell-Bloch equations for the intracavity field, polarization, and population difference are $X_c = \sqrt{3}(1+i\Delta)$, $P_c = \sqrt{3}/4$, $F_c = 1/4$, respectively. In these expressions, $\Delta = (\omega_a - \omega_e)/\gamma_\perp = -(\omega_c - \omega_e)/\kappa$ is the detuning parameter, with $\omega_a(\omega_e,\omega_c)$ being the atomic (external, cavity) frequency, $\gamma_\perp$ and κ are the atomic polarization and cavity decay rates. Near this critical point, the deviation X of the electric field from its value at the onset of bistability is shown to obey the SH equation [34], [35]

$$\frac{\partial X}{\partial t} = 4Y + X(C - X^2) - 4\Delta L_\perp X - \frac{4}{3}L_\perp L_\perp X, \quad (1)$$

where $Y = y - y_c - \sqrt{3}C/2$ and $C = c - c_c$ are the deviations from the injected field y and cooperativity c at the critical point. The Laplace operator is $L_\perp = \partial^2/\partial x^2 + \partial^2/\partial y^2$. Time has been scaled as in [34]. Equation (1) is valid only in the weak dispersion regime $\Delta << 1$. In the following, we shall refer to Y, X, and C simply as the input field, the cavity field, and the cooperativity parameter, respectively, and not as deviations from the the corresponding variables at the critical point.

The homogeneous stationary solutions X_s of (1) are given by $4Y = X_s(X_s^2 - C)$. For $C < 0\,(C > 0)$ the transmitted intensity as a function of the input intensity Y^2 is monostable (bistable). The HSS undergoes a modulational (or Turing) instability at $Y_{T\pm} = \pm(3\Delta^2 - 2C)X_{T\pm}/12$ with $X_{T\pm} = \pm\sqrt{\Delta^2 + C/3}$. At these bifurcation points, the critical wavenumber is $k_T = \sqrt{3\Delta/2}$. Thus, spontaneous pattern-forming instability requires $\Delta > 0$ and $C > -3\Delta^2$ to have k_T and $X_{T\pm}$ real. In the monostable regime, the single HSS is unstable in the range $Y_{T-} < Y < Y_{T+}$. However, when the system exhibits a bistable behavior, two portions of the upper and the lower homogeneous branches become modulationally unstable, i.e., this instability occurs in the range: $Y_{l+} < Y < Y_{T-}$ and $Y_{T+} < Y < Y_{l-}$, where $Y_{l\pm} = \pm(1/2)(C/3)^{3/2}$ at the turning points. They are saddle-node bifurcation points connecting the intermediate

branch to the upper and lower HSS, which is always unstable even in the absence of diffraction.

III. Turing and Zero-Mode Interaction

In our previous work, we have considered the monostable case by using a weakly nonlinear analysis based on an expansion in terms of a small parameter which measures the distance from the critical modulational point [12]. The amplitude equations corresponding to the various types of 2-D solutions are valid in the weakly nonlinear regime provided the modulational instability is supercritical, i.e., in the range of parameters $-\Delta^2 < C < C_{\rm sub}$ with $C_{\rm sub} = -87\Delta^2/38$. The transition from super- to sub-critical of both modulational instabilities occurs at $C = C_{\rm sub}$. This transition requires $C < 0$, which is far from the onset of bistability. For a given Δ, the classification of the different regimes of instability domains is displayed in Fig. 1, where we plot the threshold coordinates for the modulational ($Y_{T\pm}$) and the saddle-node ($Y_{l\pm}$) bifurcations as a function of the cooperativity parameter. When the Turing bifurcations are supercritical, a weakly nonlinear analysis is sufficient to construct the stable periodic solution. In this case, the amplitude of the zero mode coincides with the corresponding HSS. However, when increasing the cooperativity parameter, just before the occurrence of bistability, the Turing bifurcations are subcritical. In addition, the zero mode becomes an active mode and must be taken into account in the dynamics of the system, which modifies not only the amplitude of the 2-D structures but also their stability. For large aspect ratios, i.e., large Fresnel numbers, the distance between the nearest eigenvalues of the linearized analysis is very small, leading to a quasicontinuous spectrum of the Laplace operator. The periodic solutions may then be approximated by a superposition of plane waves with a critical wavevector $\mathbf{k}_j$, and the homogeneous zero mode

$$X(\mathbf{r},t) = R_0(t) + \sum_{j=1}^{N} R_j(t)\exp i(\mathbf{k_j}.\mathbf{r} + \phi_j) + c.c.$$

where $c.c.$ denotes the complex conjugate. The real amplitude $R_0\,(R_j)$ is the amplitude of the zero-homogeneous (Turing) mode, and ϕ_j is the phase of the mode j. The stripes and rhomboids are characterized by $N = 1$ and $N = 2$, respectively, and the hexagons are obtained for $N = 3$.

A. Stripes

We consider the simplest nonlinear solution corresponding to one transverse dimension (stripes). To calculate the solutions emerging from both modulational bifurcation points, we use a standard nonlinear analysis based on a truncated Fourier-mode expansion of the field, including the homogeneous mode. Such an analysis allows us to derive analytically amplitude equations for transverse structures and assess their stability. For the stripes, we have

$$\frac{\partial R_0}{\partial t} = 4Y + (C - R_0^2)R_0 - 6R_1^2R_0 \tag{2}$$

$$\frac{\partial R_1}{\partial t} = \mu R_1 - 3(R_0^2 + R_1^2)R_1 \tag{3}$$

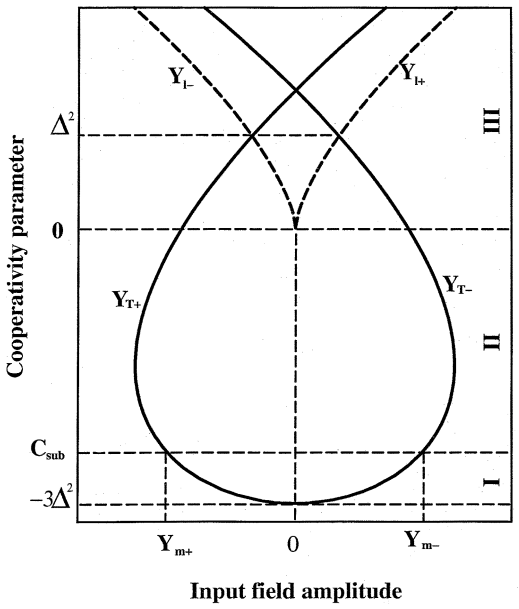

Fig. 1. Thresholds associated with the modulational instabilities $Y_{T\pm}$ are plotted (full line) as a function of cooperativity parameter. The broken curve indicate the coordinate of saddle node bifurcations $Y_{l\pm}$. The two monostable regimes I, II, correspond respectively the supercritical modulational and subcritical modulational instability. The HSS undergoes a modulational instability either at Y_{T-} when the input field is increased from below or at Y_{T+} when it is decreased from above. In domain III, the system undergoes both bistable behavior and modulational instability. The input fields at the boundary regime separating supercritical and subcritical regimes are $Y_{m\pm} = (3\Delta/19)^2\Delta\sqrt{38}$.

where $\mu = C + 3\Delta^2$. In the case of stripes, the phase equation is $\partial\phi_1/\partial t = 0$. The phase is an arbitrary constant and we therefore cancel it. Equations (2) and (3) admit two types of solutions: 1) the HSS given by $4Y + (C - R_0^2)R_0 = 0$ and $R_1 = 0$ and 2) the stripe solutions $R_0 \neq 0$ and $R_1 \neq 0$. They are given by $A_{\rm st} = \pm\sqrt{\mu/3 - R_{0\rm st}^2}$ with $4Y + (C - 2\mu + 5R_{0\rm st}^2)R_{0\rm st} = 0$. The stability analysis of the stripe structures shows that they are stable in the domain where they exist. Two typical cases are considered. First, we consider the situation where the system approaches the bistable regime corresponding to domain II in Fig. 1. The bifurcation diagram corresponding to that case is plotted in Fig. 2. The HSS undergoes a modulational instability at Y_{T-} and at Y_{T+}. From both bifurcation points, two unstable periodical solutions emerge subcritically. At the turning points $Y = Y_{L\pm}$, the unstable branches of solutions are connected to stable stripes solutions which form two continuous lines. They correspond to the extremal values of the intracavity field amplitudes $X_{\rm max,min} = R_{0\rm st} \pm 2A_{\rm st}$ plotted in Fig. 2. In addition, we plot in the same figure the average value of field amplitude, $R_{0\rm st} = (X_{\rm max} + X_{\rm min})/2$, which is the amplitude of the zero mode. Numerical simulations of (1) have been performed to compare with the analytical results. We plot in Fig. 2 the two amplitudes obtained by analytical calculation (continuous lines) and by simulations (black dots). The agreement is excellent.

Second, we consider the bistable regime corresponding to domain III in Fig. 1. In that case, we show in Fig. 3 a typical bifurcation diagram that is obtained for positive cooperativity. The thresholds associated with the modulational instability are located on the upper and lower branches of HSS. In the bistable

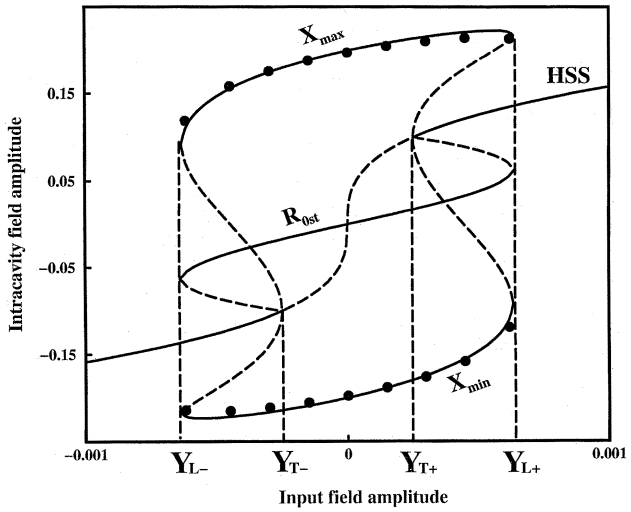

Fig. 2. 1-D monostable bifurcation diagram. Parameters are $\Delta = 0.1$ and $C = -10^{-4}$. Full (broken) curve indicates stable (unstable) maximum and minimum of the intracavity field amplitude. $X_{\pm}$ and $R_{0\mathrm{st}}$ correspond to the extrema of periodic structures and the homogeneous zero-mode amplitude, respectively. HSS denotes the homogeneous steady states. Both bifurcations appear subcritically. Black dots indicate the maximum and the minimum amplitude obtained by the numerical simulations of the full model (1).

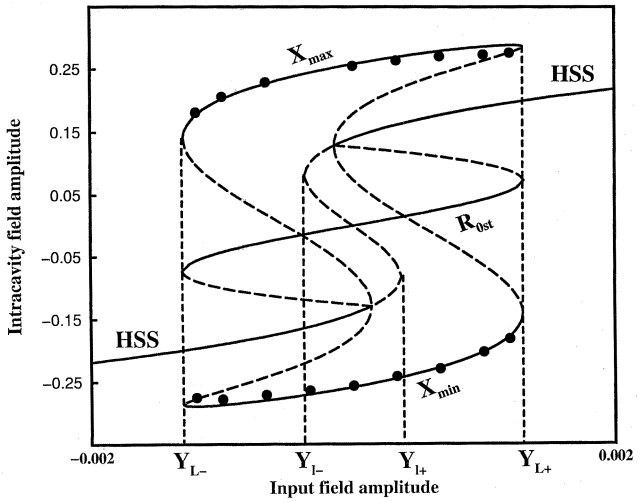

Fig. 3. 1-D bistable bifurcation diagram. Parameters are $\Delta = 0.1$ and $C = 0.02$. Full and broken curves indicate, respectively, stable and unstable maximum and minimum amplitude of the intracavity field obtained analytically. The $X_{\pm}$ and $R_{0\mathrm{st}}$ correspond to the extrema of the periodic structures and the homogeneous zero-mode amplitude, respectively. HSS denotes the homogeneous steady states. Both bifurcations appear subcritically. The black dots indicate the maximum and the minimum amplitude obtained by the numerical simulations of the full model (1).

regime, the modulational instability always appears subcritically. However, the domain of stability of periodic structures is much larger than the size of the HSS hysteresis which occurs in the domain $Y_{l-} < Y < Y_{l+}$ with $Y_{l\pm} = \pm(1/2)(C/3)^{3/2}$. This is one of the consequences of the interaction between the critical ($|\mathbf{k}| = k_T$) and the homogeneous ($|\mathbf{k}| = 0$) modes: the branch of periodic patterns extends beyond the limit points $Y = Y_{l\pm}$, up to the Turing point corresponding to periodic branches of solutions $Y = Y_{L\pm}$. As in the monostable regime, we plot in Fig. 3 the extremal values $X_{\max,\min}$ of the intracavity field amplitudes and the amplitude of the zero-homogeneous mode $R_{0\mathrm{st}}$. In that figure, the results from the numerical simulations (black dots) are also plotted and it is seen that again the agreement between numerical and analytical results is excellent.

In the weakly nonlinear regime corresponding to domain I in Fig. 1, a perturbation expansion in the vicinity of the Turing critical point can be used to construct the solutions [12]. However, an important difference appears when approaching the bistable regime: the coupling between the Turing and the quasineutral homogeneous modes allows transverse patterns to oscillate around the zero-homogeneous mode amplitude $R_{0\mathrm{st}}$.

B. Hexagons

In Section III-A, we considered only the 1-D case leading to the stripe structures. Here, we focus on the 2-D problem. The linear stability analysis is the same as in the 1-D case. An essential difference appears when considering 2-D pattern selection. At the threshold associated with modulational instability, the HSS becomes unstable with respect to transverse wavevectors that have the same modulus $k = k_T$ but have no preferred direction, since the system is isotropic in the (x, y) transverse plane. Although an indefinite number of modes may be generated with an arbitrary direction (rotational degeneracy), a regular pattern is selected and emerges due to the nonlinear interactions. Suppose that there are only two wavevectors $\mathbf{k}_{1,2}$. The two modes compete, interact, and are equally amplified due to the rotational degeneracy. Two situations can arise: 1) the combination $\mathbf{k}_1+\mathbf{k}_2$ is not resonant, i.e., $\mathbf{k}_1 + \mathbf{k}_2$ does not fall on the critical circle of radius k_T, and the dynamics can be described in terms of two modes $\mathbf{k}_1$ and $\mathbf{k}_2$ and 2) the combination $\mathbf{k}_1 + \mathbf{k}_2 = \mathbf{k}_3$ lies on the critical circle, i.e., $|\mathbf{k}_3| = k_T$, and the resonant mode $\mathbf{k}_3$ generated by the dynamics needs to be included in the analysis. This can only happen if the angle between $\mathbf{k}_1$ and $\mathbf{k}_2$ is $2\pi/3$. In the nonresonant case 1), we deal with rhombic cells, while in the resonant case 2), we have a lattice of hexagonal cells. With the SH equation, rhombic structures are intrinsically unstable. The proof of this point is similar to the instability proof of tetrahedral structures in 3-D [33]. We, therefore, focus the analysis on the resonant case corresponding to hexagonal structures. The amplitude equations are

$$\frac{\partial R_0}{\partial t} = S(R_0) - 6R_0\sum_{j=1}^{3} R_j^2 - 12R_1R_2R_3\cos\psi \quad (4)$$

$$\frac{\partial R_1}{\partial t} = \mu R_1 - 3[R_0^2 + R_1^2 + 2(R_2^2 + R_3^2)]R_1 - 6R_0R_2R_3\cos\psi \quad (5)$$

$$R_1\frac{\partial \phi_1}{\partial t} = 6R_0R_2R_3\sin(\psi) \quad (6)$$

where $S(R_0) = 4Y + (C - R_0^2)R_0$ and $\psi = \sum_{j=1}^{3}\phi_j$. The equation $S(R_0) = 0$ determines the HSS. The equations for R_2, R_3, ϕ_2, and ϕ_3 are obtained from (4)–(6) by a cyclic permutation of the indices. Equation (6) can be rewritten in terms of the variable ψ as

$$\frac{\partial \psi}{\partial t} = 6R_0\frac{R_1^2R_2^2 + R_1^2R_3^2 + R_2^2R_3^2}{R_1R_2R_3}\sin(\psi). \quad (7)$$

The stationary nontrivial solutions of the amplitude equations (4) and (5) in the case of solutions with hexagonal symmetry, i.e., $R_j = A_{\rm hex}$, $j = 1,2,3$ are given by

$$S(R_{0\rm hex}) - 18A_{\rm hex}^2 R_{0\rm hex} - 12A_{\rm hex}^3 \cos\psi_s = 0$$
$$\mu/3 - 5A_{\rm hex}^2 - R_{0\rm hex}^2 - 2A_{\rm hex}R_{0\rm hex}\cos\psi_s = 0.$$

$R_{0\rm hex}$ is the stationary solution corresponding the homogeneous zero-mode amplitude.

To study the stability of these solutions, we consider internal perturbations with hexagonal symmetry: $R_0 = R_{0\rm hex} + r_0$ and $R_j = A_{\rm hex} + a_j$, $(j = 1,2,3)$, where r_0 and a_j have the form r_0,$a_j \propto \exp(\lambda t)$. Inserting these perturbations in the real amplitude equations (4) and (5), the roots of the linearized characteristic equation are

$$\lambda_{1,2} = 6A_{\rm hex}(A_{\rm hex} + 2R_{0\rm hex}\cos\psi_s)$$
$$\lambda_{3,4} = (\xi_0 + \xi_2)/2 \pm \sqrt{(\xi_0 - \xi_2)^2 - 144\xi_1 R_{0\rm hex}A_{\rm hex}}/2$$

where $\xi_0 = C - 3R_{0\rm hex}^2 - 18A_{\rm hex}^2$, $\xi_1 = -6A_{\rm hex}(R_{0\rm hex} + A_{\rm hex}\cos\psi_s)$, and $\xi_2 = -6A_{\rm hex}(3A_{\rm hex} + 2R_{0\rm hex}\cos\psi_s)$. The steady-state solutions $\psi_s = 0$ and $\psi_s = \pi$ of (7) give rise to two types of hexagonal structures. We refer to them as $H0$ and $H\pi$ structures, respectively. The linear stability analysis with respect to perturbations that affect only the phase shows that the hexagons $H0(H\pi)$ are stable (unstable) if $R_{0\rm hex}$ is negative (positive), and unstable if $R_{0\rm hex}$ is positive (negative).

C. Stripes-Hexagons Competition and Bifurcation Diagrams

The preceding analysis has shown the existence and stability of stripes, $H0$ and $H\pi$ hexagons, with respect to internal perturbations having the symmetry of the pattern. Now we consider the relative stability analysis of stripes with respect to perturbation favoring the formation of hexagons $R_0 = R_{0\rm st} + r_0$, $A_1 = A_{\rm st} + a_1$, $A_2 = a_2$, and $A_3 = a_3$. Replacing these relations in the real amplitude equations (4) and (5) leads to a linearized problem ruled by the eigenvalues

$$\lambda_{1,2} = \zeta_3 \pm \zeta_1\cos(\psi_s),$$
$$\lambda_{3,4} = \frac{1}{2}\left[(\zeta_2 + \zeta_0) + \sqrt{(\zeta_0 - \zeta_2)^2 + 8\zeta_1^2}\right].$$

where $\zeta_0 = C - 3R_{0\rm st}^2 - 6A_{\rm st}^2$, $\zeta_1 = -6A_{\rm st}R_{0\rm st}$, $\zeta_2 = \zeta_0 + 3\Delta^2 - 3A_{\rm st}^2$, and $\zeta_3 = \zeta_0 + 3\Delta^2 - 2R_{0\rm st}^2$. The results of both stability and relative stability analyses are summarized in the bifurcation diagrams shown in Figs. 4 and 5, where we plot the maximum amplitude of the stripes $(R_{0\rm st} + 2A_{\rm st})$ and of both types of hexagons $(R_{0\rm hex} + 6A_{\rm hex})$. The results of numerical simulations of the SH equation (1) are in excellent agreement with the analytical results, as in the 1-D case. They are not added to the figures to maintain clarity.

When increasing the input field amplitude Y, the structures that appear first are the hexagons $H0$. They are stable until they lose their stability to stripes. Further increasing the input field amplitude, the stripes become unstable and we observe a transition toward the hexagons' $H\pi$ branch of solutions. When reversing the variation of the input field amplitude, the $H\pi$ hexagons remain stable until the system reaches the stripe branch. Two hysteresis loops involving stripes and hexagons $H0$ or $H\pi$ appear. This behavior is shown in Fig. 4. In Fig. 5,

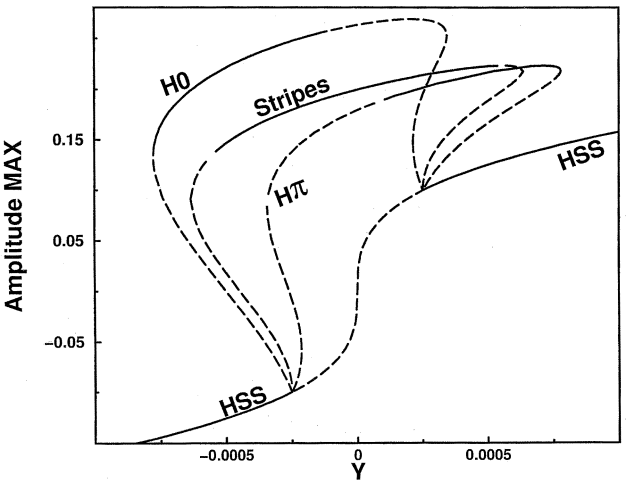

Fig. 4. 2-D monostable bifurcation diagram. Parameters are the same as in Fig. 2. The full and the broken curves indicate, respectively, stable and unstable maximum amplitude of the intracavity field obtained analytically. HSS denotes the homogeneous steady states.

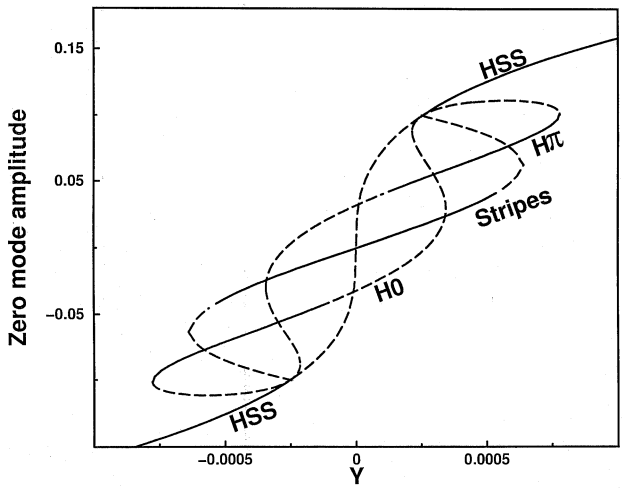

Fig. 5. 2-D monostable bifurcation diagram for the zero-mode amplitude. Same parameters as in Fig. 4. Full and the broken curves indicate stable and unstable amplitude of the homogeneous zero mode corresponding to hexagons $H0$, stripes, and $H\pi$, respectively.

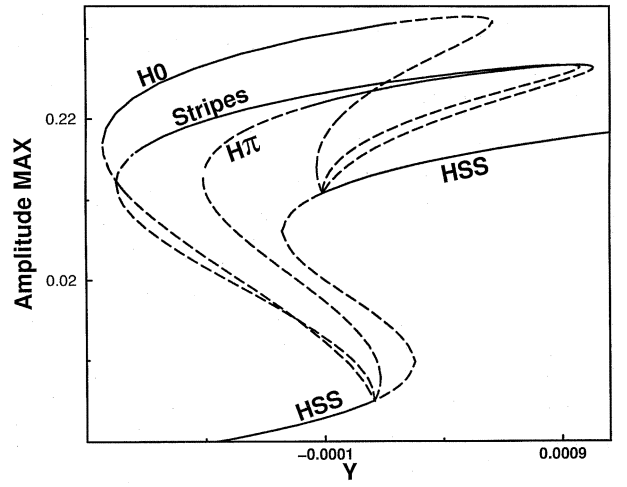

Fig. 6. 2-D bistable bifurcation diagram obtained for the same parameters as in Fig. 3. Full and broken curves indicate, respectively, stable and unstable maximum amplitude of the intracavity field obtained analytically. HSS denotes the homogeneous steady states.

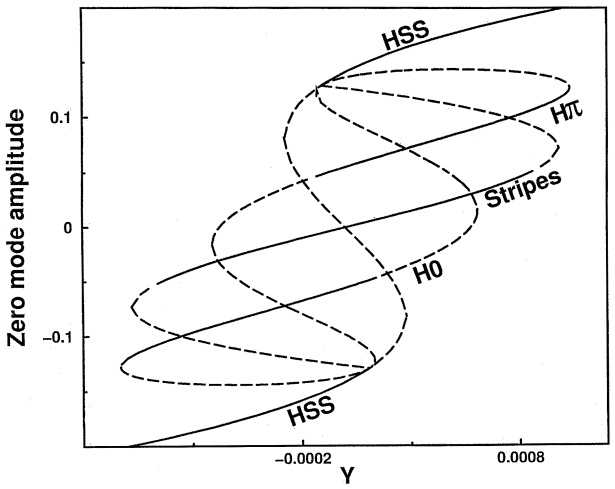

Fig. 7. 2-D bistable bifurcation diagram obtained for the same parameter as in Fig. 6. Full and the broken curves indicate, respectively, stable and unstable amplitude of the homogeneous zero mode corresponding to hexagons $H0$, stripes, and hexagons $H\pi$.

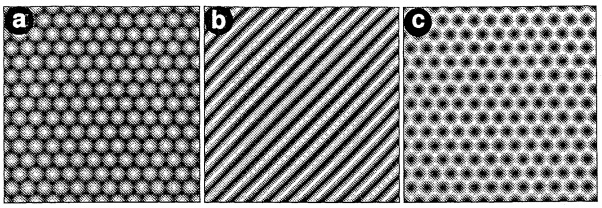

Fig. 8. 2-D periodical patterns obtained for the same value of parameters: $\Delta = 0.1$ and $C = 0.02$, and $Y = 10^{-5}$ (a) Hexagons $H0$. (b) Stripes. (c) Hexagons $H\pi$. Maxima are plain white and the mesh integration is 256×256.

we plot the amplitude of the zero mode corresponding to $H0$, stripes, and $H\pi$ of the Fig. 4. However, when considering a bistable regime, the hexagons $H0$ and $H\pi$ have an overlapping finite domain of stability as shown in Fig. 6. The amplitude of the zero mode is plotted in Fig. 7. This prediction is confirmed by the numerical integration of (1) displayed in Fig. 8, where both types of periodical structures are plotted in (x, y) the transverse plane. They are obtained for the same parameters and differ only by the initial condition.

In the domain where the two phase-locked hexagonal structures $H0$ and $H\pi$ exhibit a bistable behavior, the front between $H0$ and $H\pi$ cannot be stable for a long time. The time sequence of destabilization of that front is shown in Fig. 9. Therefore, both hexagons cannot be stable in the same transverse plane.

IV. LSs

Equation (1) admits a variety of LSs, both dark and bright, in the regime of subcritical modulational instability [43]. A sample of dark LS is displayed in Fig. 10. They are obtained by numerical integration of (1) for the same parameter values and differ only by the initial condition. *The 1-D LS are homoclinic solutions of the SH equation*. The homoclinic nature of these solutions implies that for a given set of control parameters, the number and the space distribution of both bright and dark LS immersed in the bulk of the HSS are determined only by the initial condition. LS may, therefore, be used for signal processing since the addition or the removal of a LS simply means the change

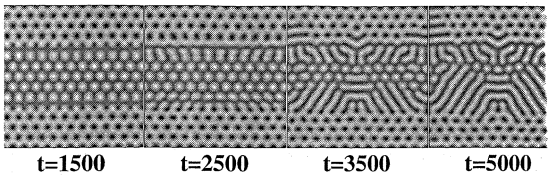

Fig. 9. Destabilization of the 2-D front connecting the two phase locked hexagonal structures obtained for the same parameters as in Fig. 8. Maxima are plain white and the mesh integration is 256×256.

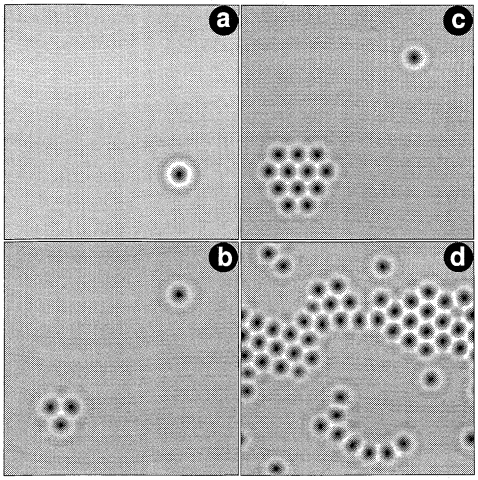

Fig. 10. Examples of 2-D localized dark LSs obtained in the monostable regime. Parameter are $\Delta = 0.1$, $C = -10^{-4}$, and $Y = 6 \times 10^{-4}$. (a) Single dark LS. (b)–(c) Self-organized LS. (d) Random distribution of dark LS. Maxima are plain white and the mesh integration is 256×256.

from one solution to another. 2-D LSs are stationary radially symmetric solutions $X(x, y) = X_0(r)$ of (1) with the cylindrical approximation $L_\perp = \partial^2/\partial r^2 + (1/r)\partial/\partial r$, and boundary conditions $dX_0(r)/dr|_{r=0} = 0$, $d^3X_0(r)/dr^3|_{r=0} = 0$, and $X_0(r) \to X_s$ at $r \to \infty$. Substituting $X(x, y) = X_s + Z(x, y)$ we obtain the equation for the deviation Z from the HSS solution

$$L(X_s)Z + N(Z) = 0 \tag{8}$$

with

$$L(X_s) = (C - 3X_s^2) - 4\Delta L_\perp - \frac{4}{3}L_\perp L_\perp \tag{9}$$

$$N(Z) = -(3X_s + Z)Z^2. \tag{10}$$

Since the localized solution $Z(x, y) = Z_0(r)$ is small for large r, its asymptotic behavior for $r \to \infty$ can be determined by solving the linearized problem which can be written as a product of two independent Helmholtz equations

$$(L_\perp + \zeta - i\xi)(L_\perp + \zeta + i\xi)Z_0 = 0 \tag{11}$$

where

$$\zeta = \frac{3\Delta}{2} \text{ and } \xi = \frac{\sqrt{3}}{2}\sqrt{3X_s^2 - C - 3\Delta^2}. \tag{12}$$

Equation (11) admits an exact solution in terms of the modified Bessel function K_0. That solution determines the asymptotic behavior of the LS

$$Z_0(r \to \infty) = \text{Re}\{Ae^{i\phi}K_0[(\gamma + i\omega)r]\} \tag{13}$$

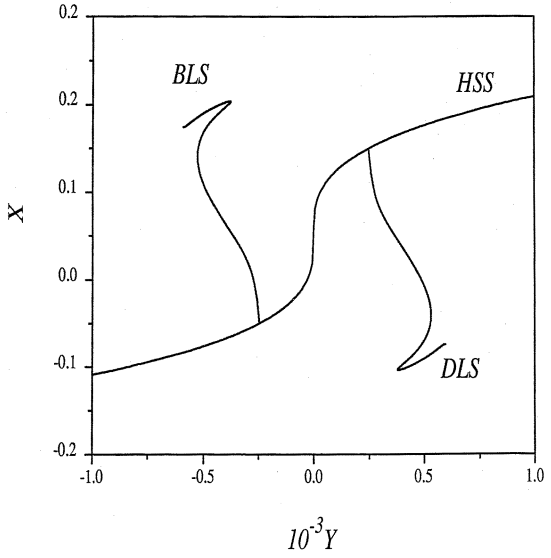

Fig. 11. 1-D monostable localized structure branches. The parameters are $\Delta = 0.1$ and $C = -10^{-4}$. Branches BLS (DLS) are the bright (dark) LSs which correspond to the maxima (minima) of the intracavity field amplitude. Curve HSS represents the spatially homogeneous solutions.

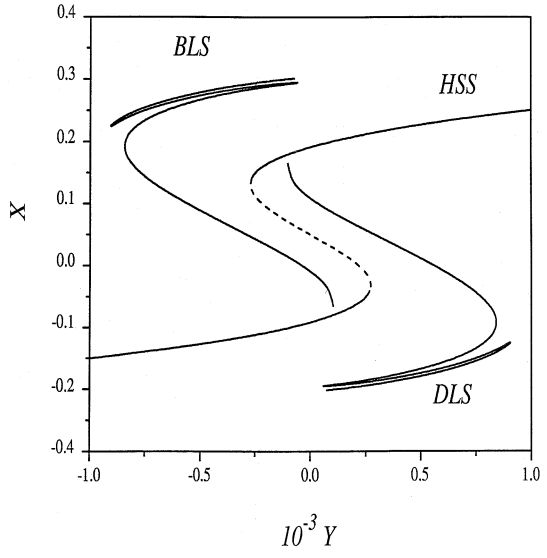

Fig. 12. 1-D bistable localized structure branches. The parameters are $\Delta = 0.1$ and $C = 0.02$. Branches BLS (DLS) are the bright (dark) LSs which correspond to the maxima (minima) of the intracavity field amplitude. The curve HSS represents the spatially homogeneous solutions.

where $\gamma + i\omega = \sqrt{-\zeta + i\xi}$ and $\gamma > 0$. The parameters A and ϕ can be obtained by asymptotically matching (13) with the solution $Z_0(r)$ calculated numerically. Let us make a connection between the parameters that appear in the expression (13) and the parameters which characterize the periodic patterns. We see that ζ is connected to the critical wavenumber at both modulational bifurcation points through the simple relation $\zeta = k_T^2$. If the parameter ξ vanishes, we have $X_{s\pm} = \pm\sqrt{\Delta^2 + C/3} \equiv X_{T\pm}$, which are exactly the intracavity amplitude thresholds associated with the modulational instability. Note that stable LS can exist only in the parameter domain where the HSS $X = X_s$ is stable. In this domain, the quantity ξ defined by (12) is real.

For large r, the Bessel function (13) can be rewritten in terms of elementary functions

$$Z_0(r \to \infty) = A\sqrt{\frac{\pi}{2r\sqrt{\gamma^2+\omega^2}}}\,\exp(-\gamma r) \times \cos\left(\omega r + \frac{1}{2}\arctan\frac{\omega}{\gamma} - \phi\right). \quad (14)$$

From this expression, we see that the LS solution Z_0 has oscillatory tail and decay for large r. The positions of the extrema of these oscillations forming a tail are determined for large r by the parameters γ, ω, and ϕ.

In order to calculate the LS solutions, we have used a procedure similar to that described in [45], [57]–[59]. First, (8) was integrated from $r = L = 50$ to $r = r_1 \sim 1$, with initial conditions defined by (13). Second, we integrated (8) from $r = r_0 = 10^{-8}$, to $r = r_1$ with the initial conditions $Z_0(r_0) = B$, $dZ_0(r)/dr|_{r=r_0} = 0$, $d^2Z_0(r)/dr^2|_{r=r_0} = C$, and $d^3Z_0(r)/dr^3|_{r=r_0} = 0$. The unknown parameters A, ϕ, B, and C are calculated by matching the two solutions at $r = r_1$. This method allows the branches of 1- and 2-D localized solutions to be drawn. The 1-D bright and dark LS branches corresponding, respectively, to one hump and one dip in the profile of the intracavity field amplitude are plotted together with the homogeneous response curves in Figs. 11 and 12. They correspond to the monostable and bistable regimes, respectively. The LS branches emerges from the modulational bifurcation points $Y_{T\pm} = \pm(3\Delta^2 - 2C)X_{T\pm}/12$ with $X_{T\pm} = \pm\sqrt{\Delta^2 + C/3}$. The bifurcation diagrams of LS corresponding to the 2-D systems are displayed in Figs. 13 and 14.

One can see from Fig. 12 that stable LS solutions can exist even beyond the limit point of the homogeneous bistability curve. This behavior is similar to periodic structures plotted in the Fig. 3. From Figs. 2 and 3 and Figs. 11 and 12, we see that the stability domains and the extremal values of periodic and LS structures are close one to another.

V. Interaction Between LSs

We have shown in Section IV that the SH equation (1) supports both dark and bright LS characterized by an oscillatory tail. In order to envisage applications of LS, a number of problems must be addressed. In particular, two or more LSs will interact through their overlapping oscillatory tails when they are close to one another. In the following, we derive analytically the potential that describes such interaction in the case of weak overlap [72], [73]. Using this result, it is possible to calculate the critical distance between LS beyond which the interaction becomes negligible.

Both bright and dark stationary LS obey the equation $L(X_s)Z_0(r) + N[Z_0(r)] = 0$, where X_s is the homogeneous steady state. Their stability is determined by the spectrum of the linear operator

$$L(Z_0(r)) = L(X_s) + \left.\frac{\partial N}{\partial Z}\right|_{Z=Z_0(r)} = L(X_s) - 3(2X_s + Z_0)Z_0$$

where $L(X_s)$ and N are defined by (9) and (10), respectively.

We consider the simplest situation corresponding to interaction between two identical radially symmetric bright LS (or two

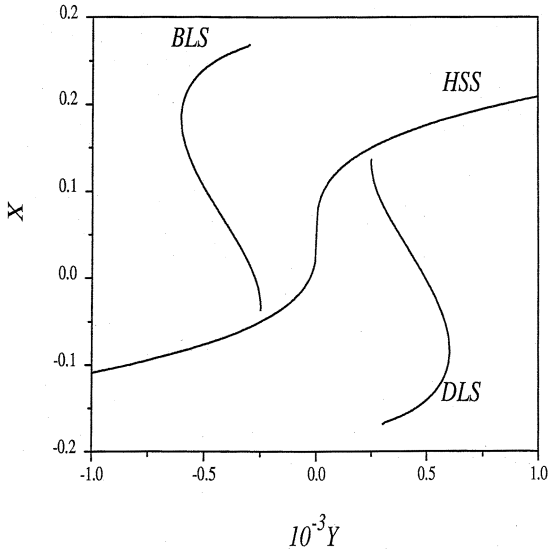

Fig. 13. 2-D monostable localized structure branches. Parameters are $\Delta = 0.1$ and $C = -10^{-4}$. Branches BLS (DLS) are the bright (dark) LSs which correspond to the maxima (minima) of the intracavity field amplitude. Curve HSS represents the spatially homogeneous solutions.

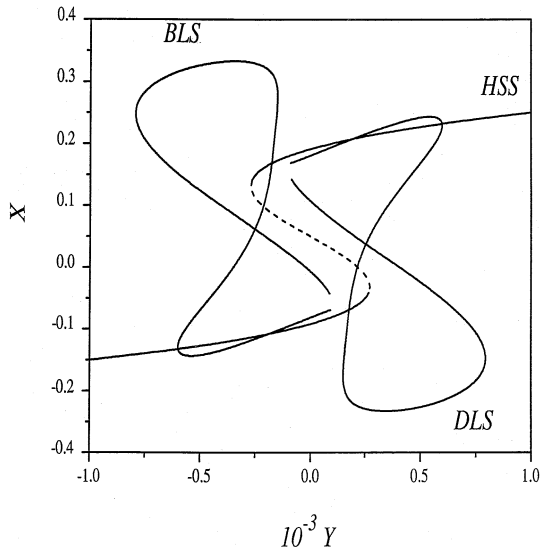

Fig. 14. 2-D bistable localized structure branches. Prameters are $\Delta = 0.1$ and $C = 0.02$. Branches BLS (DLS) are the bright (dark) LSs which correspond to the maxima (minima) of the intracavity field amplitude. Curve HSS represents the spatially homogeneous solutions.

dark LS) $Z_{1,2}(\mathbf{r}) = Z_0(\mathbf{r}-\mathbf{R}_{1,2})$ located respectively at the positions $\mathbf{R}_{1,2}$. Since the SH equation (1) admits a center of symmetry $(C,Y) = (0,0)$, corresponding to the invariance under the transformation $(C,Y) = (-C,-Y)$, we focus only on the bright LS without loss of generality. To simplify further the analysis, we assume that the maxima of the bright LS are located, respectively, at the points $(-R/2,0)$ and $(R/2,0)$ along the x direction, where $R = |\mathbf{R}| = |\mathbf{R}_2 - \mathbf{R}_1|$ is the distance between the two LSs. To study the interaction, we add a small perturbation to the linear superposition of the two LSs

$$Z(\mathbf{r},t) = Z_1(\mathbf{r}) + Z_2(\mathbf{r}) + \varepsilon\delta z(\mathbf{r},t). \tag{15}$$

We assume that the positions $\mathbf{R}_{1,2}$ of LS evolve on a slow time scale, i.e., $\mathbf{R}_{1,2} = \mathbf{R}_{1,2}(\varepsilon t)$. Inserting (15) into the SH equation (1), using the Maclaurin expansions, and equating the first-order terms in ε, we get

$$L(Z_1+Z_2)\delta z = -\frac{\partial \mathbf{R}_1}{\partial t}\cdot\nabla Z_1 - \frac{\partial \mathbf{R}_2}{\partial t}\cdot\nabla Z_2 + Q \tag{16}$$

$$Q = N(Z_1) + N(Z_2) - N(Z_1+Z_2). \tag{17}$$

To solve (16), it is necessary to satisfy the solvability condition: the right side of (16) should be orthogonal to the null eigenfunctions of the adjoint operator $L^+(Z_1+Z_2)$. Since, in our problem, the operator L is self-adjoint, $L = L^+$, the eigenfunctions of the operators $L(Z_{1,2})$ and $L^+(Z_{1,2})$ coincide. To the leading order in ε, the solvability condition is

$$\mathbf{I}_{\Omega}^{(1,2)} = \int_{\Omega} \psi_{1,2}\left[-\frac{\partial \mathbf{R}_1}{\partial t}\cdot\nabla Z_1 - \frac{\partial \mathbf{R}_2}{\partial t}\cdot\nabla Z_2 + Q\right] d\mathbf{r} = 0 \tag{18}$$

where $\psi_{1,2} = \nabla Z_{1,2}$ are the eigenfunctions of $L(Z_{1,2})$ with zero eigenvalue. These eigenfunctions correspond to the so-called translational neutral modes. The integral appearing in (18) is calculated over the $\Omega = \Re\times\Re \equiv (x,y)$-plane. To perform the integration over the domain Ω, we decompose that domain into two half-planes, namely, $\Omega_1 = \Re^-\times\Re$ and $\Omega_2 = \Re^+\times\Re$. Since the LS solution Z_2 is small in the integration domain Ω_1, we can apply the first-order Maclaurin expansion

$$\begin{aligned} N(Z_1+Z_2) &\approx N(Z_1) + Z_2\left.\frac{\partial N}{\partial Z}\right|_{Z=Z_1(\mathbf{r})} \\ &= N(Z_1) - L(X_s)Z_2 + L(Z_1)Z_2 \\ &= N(Z_1) + N(Z_2) + L(Z_1)Z_2. \end{aligned}$$

Substituting this expression into (17) and neglecting the small contribution of $\int_{\Omega_1}\nabla Z_1(\partial\mathbf{R}_2/\partial t\cdot\nabla Z_2)d\mathbf{r}$, the integral over Ω_1 becomes

$$\mathbf{I}_{\Omega_1}^{(1)} \approx \int_{\Omega_1}\nabla Z_1\left[-\frac{\partial \mathbf{R}_1}{\partial t}\cdot\nabla Z_1 - L(Z_1)Z_2\right] d\mathbf{r}.$$

A similar calculation shows that the second part of the integral is negligible, $\mathbf{I}_{\Omega_2}^{(1)} \approx 0$, since Z_1 and ∇Z_1 are small quantities in the integration domain Ω_2. Therefore, (18) leads to an expression for the velocity of the bright LS located at the position $(-R/2,0)$ in Ω_1 as follows:

$$\Gamma\frac{\partial \mathbf{R}_1}{\partial t} = -\int_{\Omega_1}\nabla Z_1 L(Z_1)Z_2 d\mathbf{r} \tag{19}$$

where $2\Gamma = \int_{\Omega_1}(\nabla Z_1)^2 d\mathbf{r} > 0$. The expression for the velocity of the LS located at $(R/2,0)$ is obtained from (19) by permutation of the indices.

By using the relation $L(Z_{1,2})\nabla Z_{1,2} = 0$ and performing an integration by parts, (19) becomes

$$\Gamma\frac{\partial \mathbf{R}_1}{\partial t} = \frac{4}{3}\left[\mathbf{S}_2 - 2(\gamma^2-\omega^2)\mathbf{S}_1\right] \tag{20}$$

with

$$\mathbf{S}_1 = -\int_{\Omega_1} (\nabla Z_1 L_\perp Z_2 - Z_2 L_\perp \nabla Z_1) d\mathbf{r},$$
$$\mathbf{S}_2 = -\int_{\Omega_1} (\nabla Z_1 L_\perp L_\perp Z_2 - Z_2 L_\perp L_\perp \nabla Z_1) d\mathbf{r}.$$

Green's theorem is used to transform the integral $\mathbf{S}_1$ into an integral over the line separating the two half planes Ω_1 and Ω_2. This line is the y axis

$$\begin{aligned}\mathbf{S}_1 &= -\int_{\Omega_1} (\nabla Z_1 L_\perp Z_2 - Z_2 L_\perp \nabla Z_1) d\mathbf{r} \\ &= -\int_{-\infty}^{\infty} \left(\nabla Z_1 \frac{\partial Z_2}{\partial x} - Z_2 \frac{\partial \nabla Z_1}{\partial x} \right) dy \\ &= \int_{-\infty}^{\infty} \frac{\partial}{\partial x} (Z_1 \nabla Z_1) dy. \end{aligned} \tag{21}$$

Here, we have used the relations

$$Z_2|_{x=0} = Z_1|_{x=0},\ \left.\frac{\partial Z_2}{\partial x}\right|_{x=0} = -\left.\frac{\partial Z_1}{\partial x}\right|_{x=0}$$
$$\nabla Z_2|_{x=0} = -\nabla Z_1|_{x=0},\ \left.\frac{\partial \nabla Z_2}{\partial x}\right|_{x=0} = \left.\frac{\partial \nabla Z_1}{\partial x}\right|_{x=0}$$

that follow from the fact that the unperturbed localized solutions Z_1 are radially symmetric and located symmetrically with respect to the y axis. Similar to (21), the integral $\mathbf{S}_2$ can be transformed into an integral over the y axis

$$\begin{aligned}\mathbf{S}_2 &= -\int_{\Omega_1} (\nabla Z_1 L_\perp L_\perp Z_2 - Z_2 L_\perp L_\perp \nabla Z_1) d\mathbf{r} \\ &= -\int_{\Omega_1} [\nabla Z_1 L_\perp L_\perp Z_2 - (L_\perp Z_2) L_\perp \nabla Z_1] d\mathbf{r} \\ &\quad -\int_{\Omega_1} [Z_2 L_\perp L_\perp \nabla Z_1 - (L_\perp Z_2) L_\perp \nabla Z_1] d\mathbf{r} \\ &= -\int_{-\infty}^{\infty} \left[\nabla Z_1 \frac{\partial L_\perp Z_2}{\partial x} - (L_\perp Z_2) \frac{\partial \nabla Z_1}{\partial x} \right] dy \\ &\quad -\int_{-\infty}^{\infty} \left[Z_2 \frac{\partial L_\perp \nabla Z_1}{\partial x} - (L_\perp \nabla Z_1) \frac{\partial Z_2}{\partial x} \right] dy \\ &= \int_{-\infty}^{\infty} \frac{\partial}{\partial x} (\nabla Z_1 L_\perp Z_1 + Z_1 L_\perp \nabla Z_1) dy. \end{aligned} \tag{22}$$

Substituting the asymptotic expression (13) of the LS into (21) and (22) and performing the integration over y, we obtain

$$\begin{aligned}&\mathbf{S}_2 - 2(\gamma^2 - \omega^2)\mathbf{S}_1 \\ &= -4\pi A^2 \gamma\omega \mathrm{Im}\{e^{2i\phi} K_0[(\gamma + i\omega)R]\}.\end{aligned}$$

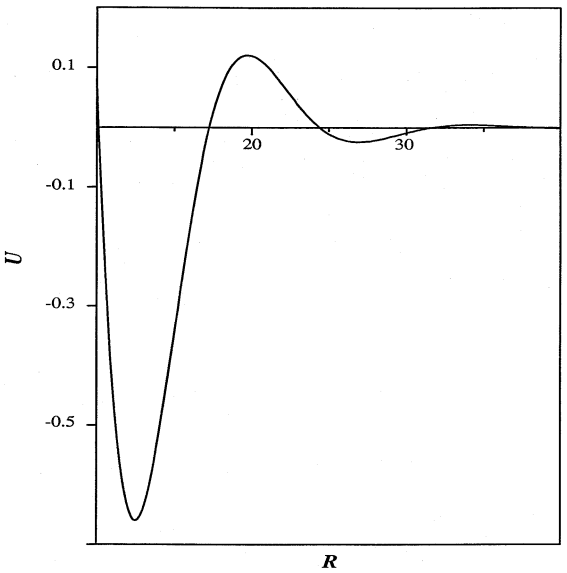

Fig. 15. Interaction potential between 2-D LSs. The parameters are $\Delta = 0.1$, $C = 0.02$, and $Y = -5 \times 10^{-4}$.

Finally, using the relation $\partial \mathbf{R}_2/\partial t = -\partial \mathbf{R}_1/\partial t$, we get

$$\frac{\partial \mathbf{R}}{\partial t} = \nabla_{\mathbf{R}} U(R)$$

with

$$U(R) = \frac{32\pi}{3\Gamma} A^2 \gamma\omega \mathrm{Im}\{e^{2i\phi} K_0[(\gamma + i\omega)R]\}. \tag{23}$$

The minima (maxima) of the interaction potential $U(R)$ correspond to stable (unstable) bound states of two LS. They are bound together by the interaction force. From (23), we see that the positions of the extrema depend on three parameters: γ, ω, and ϕ. The first two parameters are expressed analytically in terms of the parameters of the SH equation, namely, the cooperativity C and the detuning parameter Δ. The third parameter ϕ can be easily extracted from the LS solution itself. According to (13) or (14), the parameter ϕ determines the positions of the extrema of the spatial profile of LS. An example of the interaction potential is plotted in Fig. 15. Unlike the case of absorptive cavity with an injected signal [75], the construction of the interaction potential $U(R)$ for the SH equation does not require the numerical calculation of the null eigenfunction of the adjoint linear operator. Physically, the meaning of this potential is that any initial condition with two LS separated by a distance less than the distance from the origin to the first maximum leads to an asymptotic state in which the separation equal to the potential first minimum (see Fig. 15).

VI. Conclusions

In the first part of this paper, we have described pattern formation in passive systems, including the coupling between the modulational modes and the quasineutral homogeneous zero mode. We established the following analytical results: 1) the stability domains of periodic patterns are much larger than the size of the homogeneous hysteresis and 2) the interaction between modulational modes and the zero-homogeneous mode induces the coexistence of two phase-locked hexagonal structures. The

second part of the paper focused on the interaction and stability of both bright and dark LSs. We derived the interaction potential between two LSs. In particular, this determines the critical distance beyond which the interaction between two symmetric LSs becomes negligible.

ACKNOWLEDGMENT

Fruitful discussions with R. Lefever are gratefully acknowledged.

REFERENCES

[1] L. A. Lugiato and R. Lefever, "Spatial dissipative structures in passive optical systems," *Phys. Rev. Lett.*, vol. 58, pp. 2209–2211, 1987.
[2] G. Grynberg, "Mirrorless four-wave mixing oscillation in atomic vapors," *Opt. Commun.*, vol. 66, pp. 321–324, 1988.
[3] "Nonlinear optical structures, patterns, chaos," *Chaos, Solitons and Fractals*, vol. 4, pp. 1251–1844, 1994.
[4] P. Mandel, *Theoretical Problems in Cavity Nonlinear Optics*. Cambridge, U.K.: Cambridge Univ. Press, 1997.
[5] L. A. Lugiato, M. Brambilla, and A. Gatti, "Optical pattern formation," *Advances in Atomic, Molec., Opt. Phys.*, vol. 40, pp. 229–306, 1998.
[6] G. de Valcárcel, E. Roldán, and R. Vilaseca, Eds., *Quantum Semiclass. Opt*, 1998, vol. 10, pp. 775–869.
[7] G. de Valcárcel, E. Roldán, and R. Vilaseca, Eds., *J. Opt. B: Quantum Semiclass. Opt.*, 1999, vol. 1, pp. 1–197.
[8] F. T. Arecchi, S. Boccaletti, and P. L. Ramazza, "Pattern formation and competition in nonlinear optics," *Phys. Rep.*, vol. 318, pp. 1–83, 1999.
[9] W. Lange and T. Ackemann, Eds., "Complex behavior in optical systems and applications," in *J. Opt. B: Quantum Semiclass. Opt*, 2000, vol. 2, pp. 347–456.
[10] G. D'Alessandro and J. W. Firth, "Hexagonal spatial patterns for a kerr slice with a feedback mirror," *Phys. Rev. A*, vol. 46, pp. 537–548, 1992.
[11] W. J. Firth, A. J. Scroggie, G. S. McDonald, and L. A. Lugiato, "Hexagonal patterns in optical bistability," *Phys. Rev. A*, vol. 46, pp. R3609–R3612, 1992.
[12] M. Tlidi, M. Georgiou, and P. Mandel, "Transverse patterns in nascent optical bistability," *Phys. Rev. A*, vol. 48, pp. 4605–4609, 1993.
[13] M. Tlidi and P. Mandel, "Spatial patterns in nascent optical bistability," *Chaos, Solitons and Fractals*, vol. 4, pp. 1475–1486, 1994.
[14] A. J. Scroggie, W. J. Firth, G. S. McDonald, M. Tlidi, R. Lefever, and L. A. Lugiato, "Pattern formation in passive kerr cavity," *Chaos, Solitons and Fractals*, vol. 4, pp. 1323–1354, 1994.
[15] W. J. Firth and A. J. Scroggie, "Spontaneous pattern formation in an absorptive system," *Europhys. Lett.*, vol. 26, pp. 521–526, 1994.
[16] M. Tlidi, R. Lefever, and P. Mandel, "Pattern selection in optical bistability," *Quantum Semiclass. Opt.*, vol. 8, pp. 931–938, 1996.
[17] E. Pampaloni, S. Residori, and F. T. Arecchi, "Roll-hexagon transition in a kerr-like experiment," *Europhys. Lett.*, vol. 24, pp. 647–652, 1993.
[18] A. Petrossian, M. Pinard, A. Maître, J. Y. Courtois, and G. Grynberg, "Transverse patter formation for counterpropagating laser beams in rubidium vapor," *Europhys. Lett.*, vol. 18, pp. 689–694, 1992.
[19] J. B. Geddes, R. A. Indik, J. V. Moloney, and W. J. Firth, "Hexagons and squares in a passive nonlinear optical system," *Phys. Rev. A*, vol. 50, pp. 3471–3485, 1992.
[20] Y. A.Yu. A. Logvin, T. Ackemann, and W. Lange, "Subhexagons and ultrahexagons as a result of a secondary instability," *Phys. Rev. A*, vol. 55, pp. 4538–4544, 1997.
[21] G. L. Oppo, M. Brambilla, and L. A. Lugiato, "Formation and evolution of roll patterns in optical parametric oscillators," *Phys. Rev. A*, vol. 49, pp. 2028–2032, 1994.
[22] S. Longhi, "Traveling-wave states and secondary instabilities in optical parametric oscillators," *Phys. Rev. A*, vol. 53, pp. 4488–4499, 1996.
[23] C. Etrich, U. Peschel, and F. Lederer, "Pattern formation in intracavity second-harmonic generation," *Phys. Rev. E*, vol. 56, pp. 4803–4808, 1997.
[24] P. Lodahl, M. Bache, and M. Saffman, "Modification of pattern formation in doubly resonant second harmonic generation by competing parametric oscillation," *Opt. Lett.*, vol. 25, pp. 654–656, 2000.
[25] ——, "Spatiotemporal structures in the internally pumped optical parametric oscillator," *Phys. Rev. A*, vol. 63, p. 023 815, 2000.
[26] R. Kuszelewicz, I. Ganne, I. Sagnes, G. Slekys, and M. Brambilla, "Optical self-organization in bulk and multiquantum well GaAlAs microresonators," *Phys. Rev. Lett.*, vol. 84, pp. 6006–6009, 2000.
[27] S. Longhi, "Transverse patterns in a laser with an injected signal," *Phys. Rev. A*, vol. 56, pp. 2397–2407, 1997.
[28] S. Longhi and A. Geraci, "Roll-hexagon transition in an active optical system," *Phys. Rev. A*, vol. 57, pp. R2281–R2284, 1998.
[29] A. Barsella, C. Lepers, M. Taki, and P. Glorieux, "Swift-Hohenberg model of CO_2 laser with a saturable absorber," *J. Opt. B: Quantum Semiclass. Opt.*, vol. 1, pp. 64–69, 1999.
[30] M. Haelterman, S. Trillo, and S. Wabnitz, "Low dimensional modulational chaos in diffractive nonlinear cavities," *Opt. Commun.*, vol. 93, pp. 343–349, 1992.
[31] B. A. Malomed, "Patterns produced by a short-wave instability in the presence of a zero mode," *Phys. Rev. A*, vol. 45, pp. 1009–1017, 1992.
[32] G. Dewel, S. Métens, M. F. Hilali, P. Borckmans, and C. B. Price, "Resonant patterns through coupling with a zero mode," *Phys. Rev. Lett.*, vol. 74, pp. 4647–4650, 1995.
[33] M. Tlidi, M. F. Hilali, and P. Mandel, "Instability of optical tetrahedral dissipative crystals," *Europhys. Lett.*, vol. 55, pp. 26–32, 2001.
[34] P. Mandel, M. Georgiou, and T. Erneux, "Transverse effects in coherently driven nonlinear cavities," *Phys. Rev. A*, vol. 47, pp. 4277–4286, 1993.
[35] M. Le Berre, E. Ressayre, and A. Tallet, "Why does a Ginzburg-Landau diffraction equation become a diffusion equation in the passive ring cavity," *Quantum Semiclass. Opt*, vol. 7, pp. 1–4, 1995.
[36] S. Longhi and A. Geraci, "Swift-Hohenberg equation for optical parametric oscillators," *Phys. Rev. A*, vol. 54, pp. 4581–4584, 1996.
[37] G. J. de Valcárcel, K. Staliunas, E. Roldán, and V. J. Sánchez-Morcillo, "Transverse patterns in degenerate optical parametric oscillation and degenerate four-wave mixing," *Phys. Rev. A*, vol. 54, pp. 1609–1624, 1996.
[38] S. Longhi, "Spatial solitary wavesand patterns in type II second-harmonic generation," *Optics Lett.*, vol. 23, pp. 346–348, 1998.
[39] J. V. Moloney and H. M. Gibbs, "Role of diffractive coupling and self-focusing or defocusing in the dynamical switching of a bistable optical cavity," *Phys. Rev. Lett.*, vol. 48, pp. 1607–1610, 1982.
[40] W. McLaughlin, J. V. Moloney, and A. C. Newell, "Solitary waves as fixed points of infinite-dimensional maps in an optical bistable ring cavity," *Phys. Rev. Lett.*, vol. 51, pp. 75–78, 1983.
[41] J. V. Moloney and A. C. Newell, *Nonlinear Optics*. Redwood City, CA: Addison-Wesley, 1992.
[42] N. N. Rosanov, "Transverse patterns in wide-aperture nonlinear optical systems," in *Progress in Optics*. Amsterdam, The Netherlands: North-Holland, 1996, vol. 35, pp. 1–60.
[43] M. Tlidi, P. Mandel, and R. Lefever, "Localized structures and localized patterns in optical bistability," *Phys. Rev. Lett.*, vol. 73, pp. 640–643, 1994.
[44] M. Brambilla, L. A. Lugiato, and M. Stefani, "Interaction and control of optical localized structures," *Europhys. Lett.*, vol. 34, pp. 109–114, 1996.
[45] W. J. Firth and A. J. Scroggie, "Optical bullet holes: robust controllable localized states of a nonlinear cavity," *Phys. Rev. Lett.*, vol. 76, pp. 1623–1626, 1996.
[46] B. A. Samson and M. A. Vorontsov, "Localized states in a nonlinear optical system with a binary-phase slice and a feedback mirror," *Phys. Rev. A.*, vol. 56, pp. 1621–1626, 1997.
[47] C. Etrich, U. Peschel, and F. Lederer, "Solitary waves in quadratically nonlinear resonators," *Phys. Rev. Lett.*, vol. 79, pp. 2454–2457, 1997.
[48] K. Staliunas and V. J. Sanchez-Morcillo, "Localized structures in degenerate optical parametric oscillator," *Opt. Commun.*, vol. 139, pp. 306–312, 1996.
[49] S. Longhi, "Localized structures in optical parametric oscillator," *Physica Scripta*, vol. 56, pp. 611–618, 1997.
[50] P. Lodahl, M. Bache, and M. Saffman, "Spatiotemporal structures in the internally pumped optical parametric oscillator," *Phys. Rev. A*, vol. 63, p. 023 815, 2001.
[51] M. Brambilla, L. A. Lugiato, F. Prati, L. Spinelli, and W. J. Firth, "Spatial soliton pixels in semiconductor devices," *Phys. Rev. Lett.*, vol. 79, pp. 2042–2045, 1997.
[52] L. Spinelli, G. Tissoni, M. Brambilla, F. Prati, and L. A. Lugiato, "Spatial solitons in semiconductor microcavities," *Phys. Rev. A*, vol. 58, pp. 2542–2559, 1998.
[53] G. Tissoni, L. Spinelli, L. Brambilla, T. M. Maggipinto, I. M. Perrini, and L. A. Lugiato, "Cavity solitons in passive bulk semiconductor microcavities. I. microscopic model and modulational instabilities," *J. Opt. Soc. Amer. B*, vol. 16, pp. 2083–2094, 1999.

[54] T. Maggipinto, M. Brambilla, G. K. Harkness, and W. J. Firth, "Cavity solitons in semiconductor microresonators: existence, stability, and dynamical properties," *Phys. Rev. E*, vol. 62, pp. 8726–8739, 2000.
[55] Y. A.Yu. A. Logvin and T. Ackemann, "Interaction between Hopf and static instabilities in a pattern-forming optical system," *Phys. Rev. E*, vol. 58, pp. 1654–1661, 1998.
[56] R. Vilaseca, M. C. Torrent, J. Garcia-Ojalvo, M. Brambilla, and M. San Miguel, "Two-photon cavity solitons in active optical media," *Phys. Rev. Lett.*, vol. 87, p. 083 902, 2001.
[57] A. G. Vladimirov, N. N. Rosanov, S. V. Fedorov, N. A. Kaliteevskii, and G. V. Khodova, "Bifurcation analysis of laser autosolitons," *Quantum Electron.*, vol. 27, pp. 949–952, 1997.
[58] A. G. Vladimirov, N. N. Rosanov, S. V. Fedorov, and G. V. Khodova, "Analysis of the stability of laser solitons," *Quantum Electron.*, vol. 28, pp. 55–57, 1998.
[59] A. G. Vladimirov, N. A. Fedorov, S. V. Kaliteevskii, G. V. Khodova, and N. N. Rosanov, "Numerical investigation of laser localized structures," *J. Opt. B: Quantum Semiclass. Opt.*, vol. 1, pp. 101–106, 1999.
[60] M. Tlidi, P. Mandel, and M. Haelterman, "Spatiotemporal patterns and localized structures in nonlinear optics," *Phys. Rev. E*, vol. 56, pp. 6524–6530, 1997.
[61] M. Tlidi and P. Mandel, "Space-time localized structures in the degenerate optical parametric oscillator," *Phys. Rev. A*, vol. 59, pp. R2575–R2578, 1999.
[62] D. V. Skryabin and W. J. Firth, "Interaction of cavity solitons in degenerate optical parametric oscillators," *Opt. Lett.*, vol. 24, pp. 1056–1058, 1999.
[63] D. V. Skryabin, "Instabilities of cavity solitons in optical parametric oscillators," *Phys. Rev. E*, vol. 60, pp. R3508–R3511, 1999.
[64] A. Barsella, C. Lepers, and M. Taki, "Transverse wave number selection and propagation of 2D-pulses in lasers with saturable absorber," *Opt. Commun.*, vol. 181, pp. 401–406, 2000.
[65] M. Le Berre, S. Patrascu, E. Ressayre, and A. Tallet, "Localized structures in chaotic patterns: from disorder to ordering," *Phys. Rev. A*, vol. 56, pp. 3150–3160, 1997.
[66] V. B. Taranenko, I. Ganne, R. Kuszelewicz, and C. O. Weiss, "Patterns and localized structures in bistable semiconductor resonators," *Phys. Rev. A*, vol. 61, p. 063 818, 2000.
[67] G. Slekys, I. Ganne, I. Sagnes, and R. Kuszelewicz, "Optical pattern formation in passive semiconductor microresonators," *J. Opt. B: Quantum Semiclass. Opt.*, vol. 2, pp. 443–446, 2000.
[68] V. B. Taranenko, C. O. Weiss, and W. Stols, "Semiconductor resonator solitons above bandgap," *J. Opt. Soc. Amer. B*, vol. 19, pp. 684–688, 2002.
[69] P. L. Ramazza, S. Ducci, S. Boccaletti, and F. T. Arecchi, "Localized versus delocalized patterns in a nonlinear optical interferometer," *J. Opt. B: Quantum Semiclass. Opt.*, vol. 2, pp. 399–405, 2000.
[70] Y. A.Yu. A. Logvin, B. Schäpers, and T. Ackemann, "Stationary and drifting localized structures near a multiple bifurcation point," *Phys. Rev. E*, vol. 61, pp. 4622–4625, 2000.
[71] B. Schäpers, M. Feldmann, T. Ackemann, and W. Lange, "Interaction of localized structures in an optical pattern-forming system," *Phys. Rev. Lett.*, vol. 85, pp. 748–751, 2000.
[72] K. A. Gorshkov and L. A. Ostrovsky, "Interaction of solitons in non integrable systems: direct perturbation method and applications," *Physica D*, vol. 3, pp. 428–438, 1981.
[73] I. S. Aranson, K. A. Gorshkov, A. S. Lomov, and M. I. Rabinovich, "Stable particle-like solutions of multidimensional nonlinear fields," *Physica D*, vol. 43, pp. 435–453, 1990.
[74] A. G. Vladimirov, G. V. Khodova, and N. N. Rosanov, "Stable bound states of one-dimensional autosolitons in a bistable laser," *Phys. Rev. E*, vol. 63, p. 056 607, 2001.
[75] A. G. Vladimirov, J. O. McSloy, D. V. Skryabin, and W. J. Firth, "Two-dimensional clusters of solitary structures in driven optical cavities," *Phys. Rev. E*, vol. 65, p. 046 606, 2002.

Mustapha Tlidi was born in Morocco. He received the M.D. and Ph.D. degrees in physics from the science faculty of the Université Libre de Bruxelles (uLB), Brussels, Belgium, in 1989 and 1995, repectively.

From 1995 to 2002, he held a temporary position in the Service d'optique Nonlinéaire Théorique, uLB. Since October 2002, he has held a tenured position with the Belgian National Science Foundation. His research is focused on diffractive nonlinear optics in two or three dimensions, including transverse pattern formation, chromatic dispersion effect, localized structures or cavity solitons (stability and interaction), three-dimensional dissipative optical crystals and light drops, domain growth in nonlinear optics, and space-time instabilities in passive and active devices.

Dr. Tlidi is a member of the Optical Society of America.

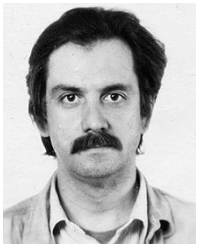

Andrei G. Vladimirov was born in Leningrad (now St. Petersburg), Russia, in 1958. He received the Ph.D. degree from Leningrad State University, Leningrad, Russia, in 1984.

He is currently an Associate Professor in the Department of General Physics, St. Petersburg State University, St. Petersburg, Russia. His research interests include nonlinear dynamics in lasers and laser systems, localized structures of light, optical solitons.

Dr. Vladimirov is a member of the Russian Optical Society.

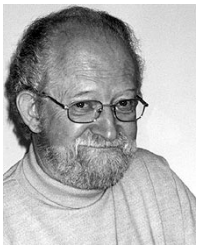

Paul Mandel (M'89) was born in Geneva, Switzerland, in 1942. He received the M.D. degree in 1965, the Ph.D. degree in 1969, and the Thèse d'agrégation in 1980, all from the Université Libre de Bruxelles, Brussels, Belgium.

He is with the National Fund for Scientific Research (Belgium) and also with the Theoretical Nonlinear Optics Group, Université Libre de Bruxelles, Bruxelles, Belgium, where he is currently teaching nonlinear optics and quantum optics in the Science and Applied Science faculties. Since 1972, his research topics have been in the field of quantum and semiclassical optics, with contributions to the theory of stability in lasers (gas, solid state, and semiconductor lasers), optical bistability and $\chi^{(2)}$ nonlinear media, including time-dependent control parameters, multimode dynamics and transverse effects.

He is a Fellow of the Optical Society of America.